Nanoscale Advances

ROYAL SOCIETY OF CHEMISTRY

PAPER

View Article Online
View Journal | View Issue

Cite this: *Nanoscale Adv.*, 2024, **6**, 5069

Cellular uptake and viability switching in the properties of lipid coated carbon quantum dots for potential bioimaging and therapeutics†

Sweny Jain,‡[a] Nidhi Sahu,‡[b] Dhiraj Bhatia *[a] and Pankaj Yadav*[a]

Received 11th April 2024
Accepted 5th August 2024

DOI: 10.1039/d4na00306c

rsc.li/nanoscale-advances

Carbon quantum dots derived from mango leaves exhibited red fluorescence. These negatively charged particles underwent coating with the positively charged lipid molecule *N*-[1-(2,3-dioleyloxy)propyl]-*N*,*N*,*N*-trimethylammonium chloride (DOTMA). However, the bioconjugate displayed reduced uptake compared to the standalone mQDs in cancer cells (SUM 159A), and increased uptake in case of non-cancerous (RPE-1) cells. Upon *in vitro* testing, the bioconjugate demonstrated a mitigating effect on the individual toxicity of both DOTMA and mQDs in SUM-159 (cancerous cells). Conversely, it exhibited a proliferative effect on RPE-1 (normal cells).

1. Introduction

Carbon quantum dots (CQDs) are particles that exist in zero dimensions; they are nano-sized semiconductor crystals generally with a size below 10 nanometers.[1,2] Quantum dots (QDs) exhibit distinctive optical characteristics, including a narrow emission peak, a broad excitation spectrum, and robust resistance to photobleaching.[3] These unique optical properties have drawn considerable attention, especially in the realm of biomedical applications.[4,5] They are a type of carbon-based fluorescent nanomaterial. The attributes of CQDs have been harnessed for applications in the field of nanomedicine, specifically in gene therapy, drug delivery, photothermal and radiotherapy, diagnostic techniques, biosensing, the development of fluorescent nanoprobes for bioimaging, and bactericidal activities.[6,7] These materials have attracted growing interest in recent years, primarily because of their exceptional qualities, including environment-friendliness, cost-effectiveness, and optical fluorescence along with low toxicity, photostability, biocompatibility, extensive surface area, high electrical conductivity, and abundant surface functional groups.[8,9]

Lipids are pivotal to biological systems, as fundamental structural and functional components of cellular membranes. Predominantly constituting the phospholipid bilayer, these amphipathic molecules create a dynamic, semi-permeable barrier that regulates the selective exchange of ions, nutrients, and signaling molecules between the intracellular and extracellular environments. Lipids, particularly phospholipids, cholesterol, and glycolipids, contribute to membrane fluidity, asymmetry, and membrane protein functionality.[10]

Beyond structural roles, lipids significantly enhance cellular uptake mechanisms. The fluidic nature of the lipid bilayer, driven by van der Waals forces among the acyl chains of fatty acids, facilitates lateral and transverse diffusion of lipid molecules and associated bioactive compounds across the membrane.[11,12] This intrinsic property is harnessed in biomedical applications, wherein lipid-based nanocarriers, such as liposomes and lipid nanoparticles, are employed to encapsulate and deliver therapeutic agents—including small molecule drugs, nucleic acids, and proteins—into cells with high efficiency.[13] Lipids enable the encapsulation of hydrophilic molecules within their aqueous core and hydrophobic molecules within the lipid bilayer, thus protecting the cargo from enzymatic degradation and improving its bioavailability. By combining biocompatibility with effective cellular internalization, lipids play an indispensable role in advancing targeted drug delivery systems and enhancing therapeutic outcomes.[14,15]

Cationic-surface L-SPIOs (superparamagnetic iron oxide nanoparticles) with an average size of 46 nm were found to exhibit enhanced cellular uptake in HeLa, PC-3, and Neuro-2a cells. *In vivo* imaging in Balb/c mice injected with CT-26 tumor cells loaded with SPIOs allowed for tracking of tumor growth using optical and MR images.[16] A study exploring lipid–polymer hybrid nanoparticles composed of PLGA coated with DOTMA and loaded with mRNA-mCherry demonstrated their significantly higher transfection efficiency (80%) compared to chitosan-PLGA NPs (5%) *in vitro*. Translation of mCherry protein within DCs was evaluated.[17] In other research, silica

[a]*Department of Biological Sciences and Engineering, Indian Institute of Technology Gandhinagar, Palaj, Gujarat 382355, India. E-mail: dhiraj.bhatia@iitgn.ac.in; yadav_pankaj@iitgn.ac.in*

[b]*Department of Bioengineering and Biotechnology, Birla Institute of Technology, Mesra Ranchi, Jharkhand-835 215, India*

† Electronic supplementary information (ESI) available. See DOI: https://doi.org/10.1039/d4na00306c

‡ These authors contributed equally.

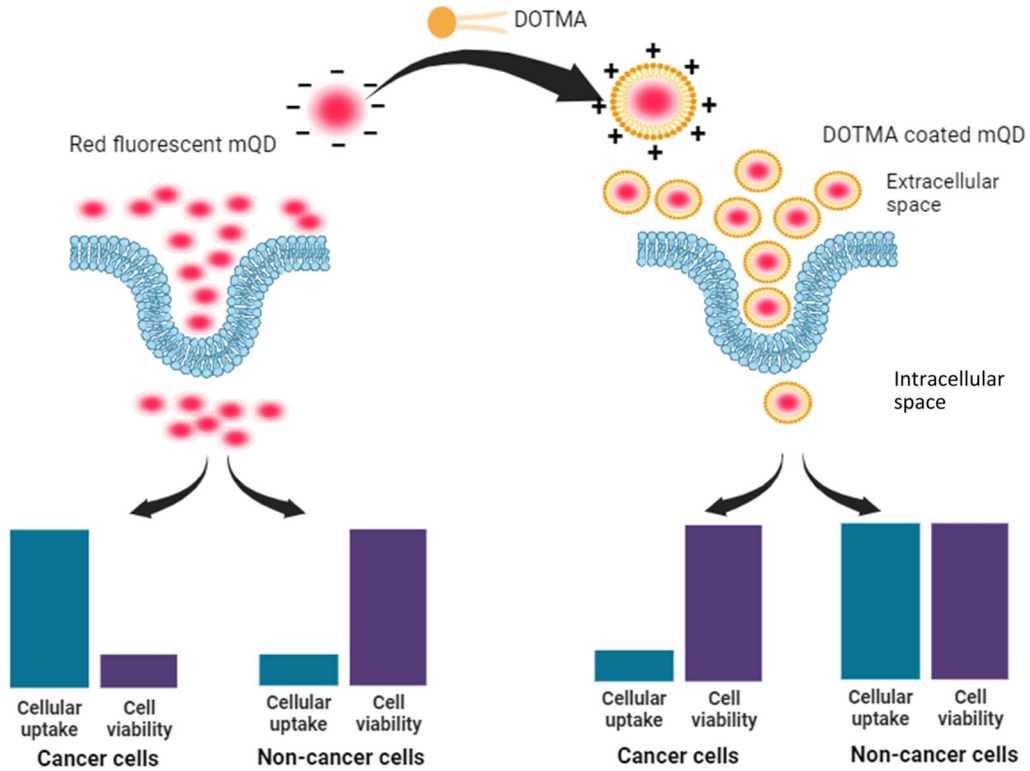

Fig. 1 mQDs coated with DOTMA increase the cell viability in both cancerous (SUM-159A) and non-cancerous (RPE-1) cells; however, the uptake is switched from higher to lower in cancer cells and from lower to higher in non-cancerous cells, which can be used for biomedical applications.

nanoparticles were double coated with PG and DOPC and were compared to uncoated nanoparticles for cellular uptake and adsorption on hybrid bilayer membranes. The lipid-coated nanoparticles showed reduced aggregation, leading to smaller structures compared to uncoated nanoparticles.[18] Further, cationic magneto liposomes with iron oxide cores and enveloped in a bilayer containing cationic lipids were studied for toxicity. Higher doses of cationic lipid were found to potentially limit uptake efficiency due to increased electrostatic attraction to the cell membrane.[19]

In recent times, the drug delivery community has shown significant interest in green synthesis of nanoparticles because they are biocompatible and environmentally friendly. The mango leaf quantum dots have been used in bioimaging and drug delivery while exhibiting low cytotoxicity compared to heavy metal QDs.[1,20] In addition, the mango leaf has antioxidant and anti-inflammatory properties which provided added benefits in quantum dots.[21] Surface modifying the lipid-coated nanoparticles due to their outstanding biocompatibility, effective permeation enhancement, and scalability allows a broad range of applications. However, the uptake of cationic lipid-coated nanoparticles is influenced by various factors, including the lipid's properties, surface decoration, size, and physicochemical attributes of liposome formulations. These elements collectively impact the potential release of cationic lipids from the nanoparticle and its subsequent movement toward the cell plasma membrane.[19,22]

In our study, we introduce novel red-emitting carbon dots, mQDs, derived from mango leaves, with an emission wavelength of 670 nm and a size of 10.1 nm. These mQDs were decorated with a small cationic lipid, *N*-[1-(2,3-dioleyloxy) propyl]-*N*,*N*,*N*-trimethylammonium chloride (DOTMA), forming a bioconjugate, mQDs : DOTMA, which exhibited enhanced fluorescence intensity, photostability, and reduced cytotoxicity compared to standalone mQDs and DOTMA. Our findings highlight the bioconjugate's potential for bioimaging, offering brighter signals and improved biocompatibility for precise cellular imaging in *in vitro* studies. Cellular internalization assays and viability assessments revealed decreased uptake in cancer (SUM159A) and increased uptake in retinal pigment epithelial (RPE-1) cells, demonstrating the bioconjugate's promising utility in cellular imaging and potential therapeutic applications (Fig. 1).

2. Materials and methods

2.1. Materials

Mango leaves were obtained from mango trees at the IIT Gandhinagar campus. Silicon oil was purchased from X-chemicals and ethanol (>99.9%) from Changshu Hongsheng Fine Chemicals Co. Ltd. The filter of 0.22 micrometer was purchased from Merck, and deionized water was obtained from a Merck Millipore system. Cationic lipid *N*-[1-(2,3-dioleyloxy)propyl]-*N*,*N*,*N*-trimethylammonium chloride (DOTMA) was purchased from

Avanti Polar Lipids. Phalloidin was purchased from Sigma Aldrich. The cell culture dishes, dimethyl sulfoxide (DMSO) and rhodamine B were purchased from Himedia. DMEM (Dulbecco's modified Eagle's medium), Ham's F12 media, FBS (fetal bovine serum), and trypsin–EDTA (0.25%) were obtained from Gibco. All the purchased chemicals were of analytical grade and did not need further purification.

2.2. Methods

2.2.1. Synthesis of mQDs. The mango leaves were plucked from a mango tree in the IIT Gandhinagar campus. Later, these leaves were washed and dried at ambient temperature for ten days. These dried leaves were then ground to form a fine powder. Next, the mango leaves and ethanol were taken in a ratio of 1 : 10 (w/v) and kept stirring for 4 hours. This mixture was then centrifuged at 10 000 rpm for 10 minutes at 25 °C. The supernatant was then refluxed for 2 hours at 160 °C. Once the solution had cooled, mQDs were obtained. Next the solvent was removed using a rotary evaporator. The mQDs were further characterized and functionalised with DOTMA to study their effects *in vitro*.

2.2.2. Characterization of mQDs. mQDs were analyzed with respect to their optical properties using both UV-Vis absorbance and fluorescence emission using Spectrocord-210 Plus Analytokjena (Germany) and FP-8300 Jasco spectrophotometers (Japan) respectively.

For AFM sample preparation mica sheets were peeled freshly and 5 μL of samples (1 : 0.25–1 : 10) having a concentration of 100 μg mL^{-1} were dropped. The sheet containing samples were then placed in a desiccator for drying overnight. Finally, the AFM imaging was done in tapping mode using a Bruker AFM instrument.

FTIR spectra of all the concentrations of mQD : DOTMA were recorded from 450 cm^{-1} to 4000 cm^{-1} using a Spectrum Two spectrometer from PerkinElmer in ATR mode. Further, analysis of the powder was done to obtain the XRD diffraction pattern using a Bruker-D8 Discover with a speed of 0.2 min^{-1} from 5° to 90°.

A Malvern Panalytical Zetasizer Nano ZS was utilized to conduct Dynamic Light Scattering (DLS) for the solution-based size characterization of mQDs and mQDs : DOTMA. Subsequently, the obtained data was plotted using a Gaussian fit in the OriginPro software.

The photostability of mQDs was analysed by incubating the samples for a duration of 10 days. Fluorescence intensity readings at 670 nm were taken every day following excitation with 400 nm light. The relative fluorescence intensity was plotted by normalizing each fluorescence intensity measurement against the maximum fluorescence intensity recorded.

These mQDs and mQD : DOTMA conjugates were then dissolved in the serum free media to assess the cellular uptake and cellular uptake of these particles in a breast cancer cell line (SUM-159A) and healthy cells (RPE-1).

2.2.3. Cell culture and cellular uptake assay. For the cellular uptake experiment, the RPE1 cells were cultured in DMEM, and SUM-159A (breast cancer) cells were maintained in HAMS-F12 media containing 10% fetal bovine serum and

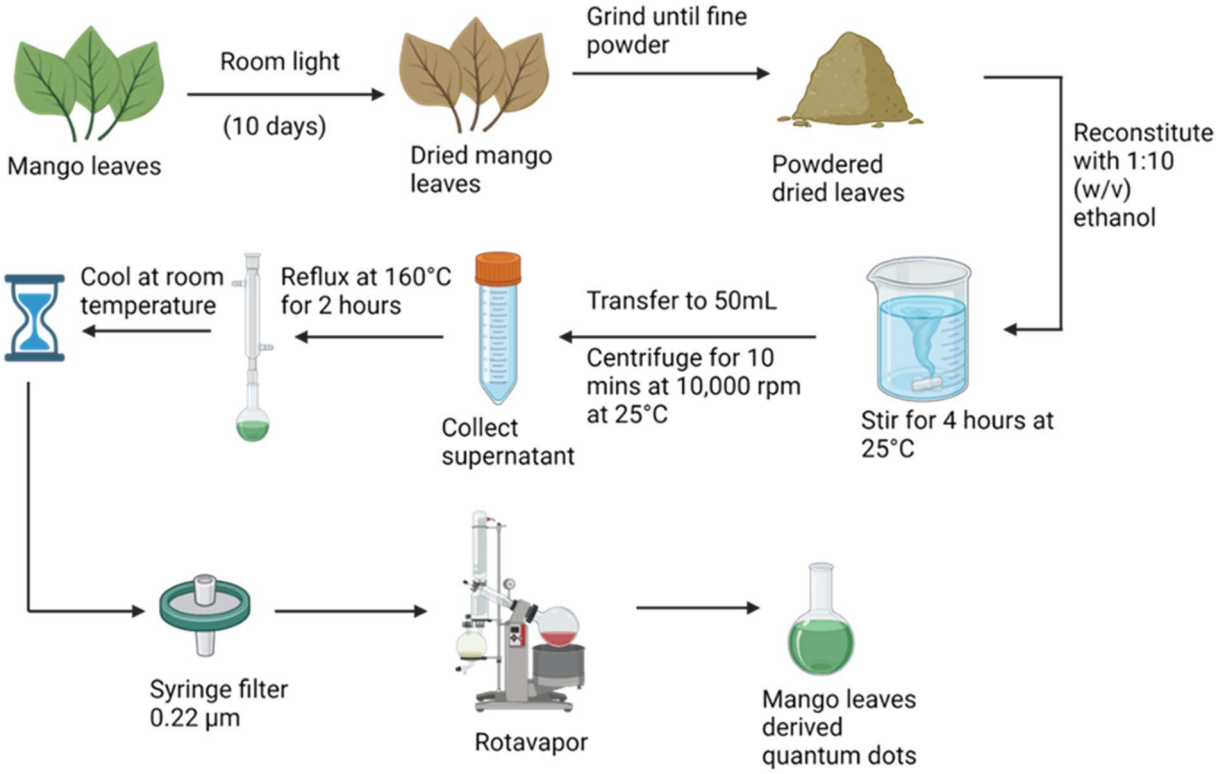

Fig. 2 Synthesis of mango leaf derived quantum dots (mQDs).

antibiotic at 37 °C with 5% CO_2 in a humidified incubator. Approximately 10^5 cells per well were seeded on a glass coverslip in a 24-well plate overnight. Before treatment, the seeded cells were washed with 1× PBS buffer three times and then incubated in serum-free media for 15 min at 37 °C with 5% CO_2 in a humidified incubator. After washing, the cells were treated with mQD and mQD : DOTMA to assess their cellular internalization. Different combinations of mQD–DOTMA (mQD : DOTMA; 1 : 0.25, 1 : 0.5, 1 : 1, 1 : 2, 1 : 5, and 1 : 10) were used for cell treatment. The treated cells were fixed for 15 min at 37 °C with 4% paraformaldehyde and rinsed three times with 1× PBS. The cells were then permeabilized with 0.1% Triton-X100 and stained with 0.1% phalloidin to visualize the actin filaments. Then the cells were washed three times with 1× PBS and mounted onto the slides with Mowiol and DAPI to stain the nucleus.

2.2.4. MTT assay. An MTT assay was performed to assess the effect of cytotoxicity of the synthesized mQD–DOTMA. Cells were seeded in 96-well plates at a seeding density of 5000 cells per well. The culture plates were incubated at 37 °C for 24 h. The cells were treated with different ratios of mQD–DOTMA (1 : 0.5, 1 : 1, 1 : 2, 1 : 5, and 1 : 10) at varied concentrations (100 μg mL^{-1}, 200 μg mL^{-1}, and 300 μg mL^{-1}). Then they were incubated at 37 °C for 24 h. Untreated cells served as a control. After incubation, a 0.5 mg mL^{-1} 3-(4,5-dimethylthiazol-2-yl)-2,5-diphenyltetrazolium bromide (MTT) solution was added to each well and incubated at 37 °C for 4 h. The solution was removed and replaced with dimethyl sulfoxide (DMSO) in each well and incubated in the dark for 15 min to dissolve the formazan crystal. A multiwell microplate reader was used to measure absorbance at 570 nm. The experiment was conducted in triplicate, with normalization to the corresponding well containing DMSO. The untreated mQDs well served as the control to determine the % cell viability of each well. The cell viability percentage was calculated using the following formula:

Cell viability (%) = Absorbance of the sample/Absorbance of the control × 100.

2.2.5. Confocal imaging. Confocal imaging was conducted on fixed cells (using a 63× oil immersion objective) and fixed tissues/embryos (using a 10× objective) employing a Leica TCS

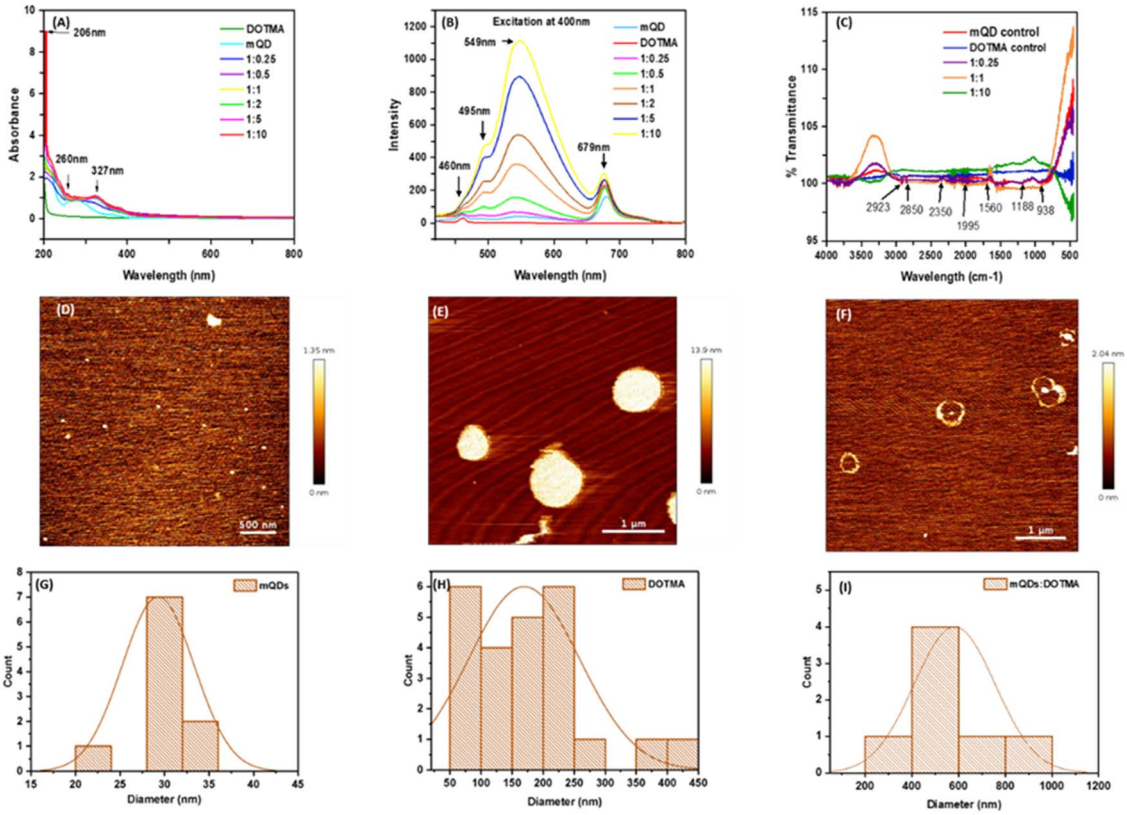

Fig. 3 Characterization of the conjugate formed of mQDs and DOTMA. (A) The UV spectra of the DOTMA showed no peaks, whereas peaks were observed in case of mQDs at 206 nm (–OH group) and 260 nm (flavonoids), and the mQD : DOTMA conjugate displayed both the peaks of mQDs and another peak at 327 nm. (B) Fluorescence spectra of DOTMA showed a peak at 460 nm, and the mQDs and mQD : DOTMA conjugate displayed peaks at 460 nm, 495 nm, 549 nm and 679 nm upon excitation at 400 nm. (C) The FTIR spectra show the presence of different functional groups present on the surface of mQDs: 2923 cm^{-1} for alkanes and acidic groups; 2850 cm^{-1} for aldehyde, alkanes, and acidic groups; 1560 cm^{-1} for nitro compounds; 1188 cm^{-1} for anhydride (acyl), amines, alcohol (alkoxy), and esters; and 938 cm^{-1} for alkenes (sp^2 C–H). (D) The quasi-spherical morphology and topography of mQDs were studied using atomic force microscopy (AFM). (E) The quasi-spherical morphology and topography of DOTMA were studied using atomic force microscopy (AFM). (F) The ring-like structure of the DOTMA coating around the mQD can be observed using atomic force microscopy (AFM). (G) Histogram plot of AFM analysis of mQDs showing their size at around 29 nm. (H) Histogram plot of AFM analysis of DOTMA showing their size at around 173 nm. (I) Histogram plot of AFM analysis of the mQD : DOTMA conjugate showing their size at around 580 nm.

SP8 confocal laser scanning microscope (CLSM) from Leica Microsystems, Germany. Various fluorophores were excited using different lasers: DAPI (405 nm) and mQDs (633 nm). The pinhole aperture was maintained at 1 airy unit throughout the imaging process. Quantitative analysis of the images was carried out using Fiji ImageJ software. The analysis involved measuring the whole cell intensity from maximum intensity projections, subtracting the background, and normalizing the measured fluorescence intensity against unlabeled cells. Approximately 40–50 cells were quantified from the collected z-stacks for each experimental condition.

2.2.6. Statistical analysis. GraphPad Prism software (version 8.0.2) was employed for statistical analysis. Data were presented as means ± standard deviation (SD) or means ± standard error from two independent experiments. p values were computed using one-way ANOVA and two-tailed unpaired Student's t-tests, with a 95% confidence interval.

3. Results

3.1. Characterization of mQDs and mQDs : DOTMA

Red fluorescence carbon quantum dots were obtained using mango leaf powder. Freshly plucked mango leaves were dried in room light. The dried mango leaves were stirred with ethanol in a 1 : 10 (weight/volume) ratio. The supernatant was then refluxed at 160 °C for 2 hours, and then filtered using a 0.22 μm

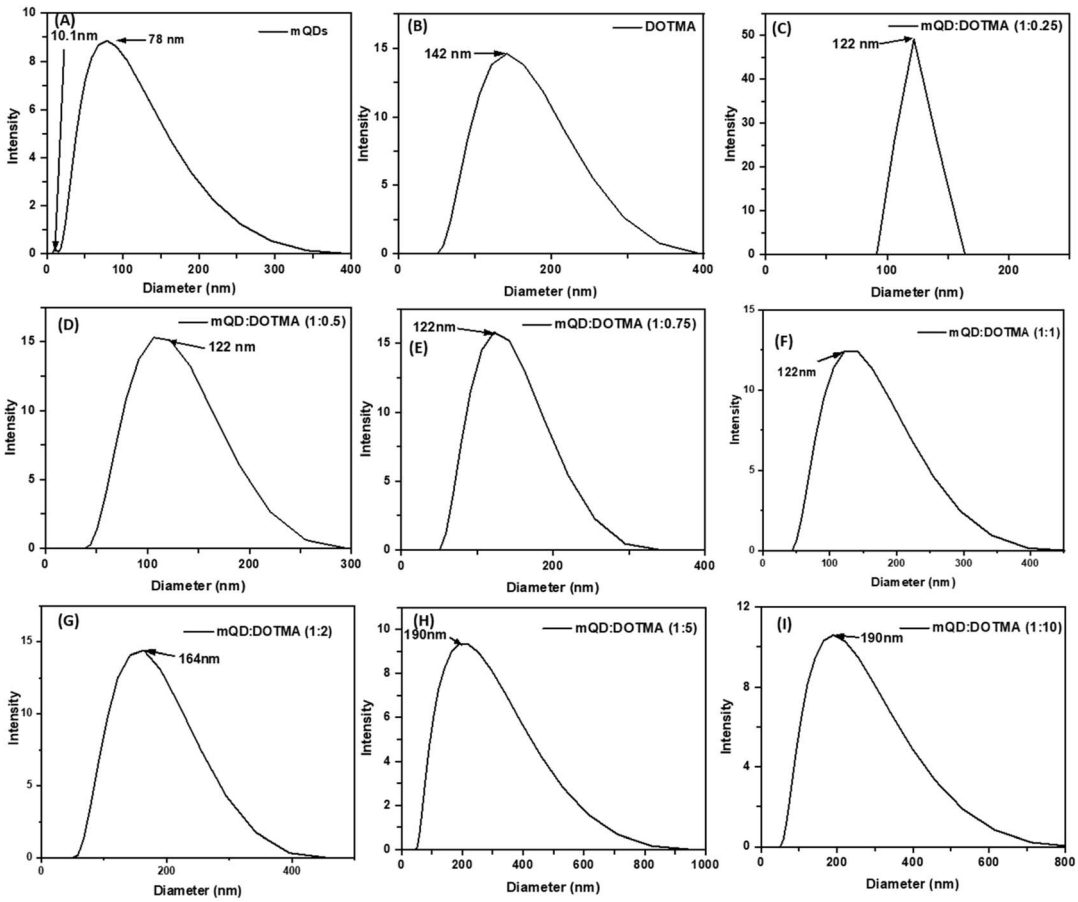

(J)

Ratios mQD:DOTMA	mQD	DOTMA	1:0.25	1:0.5	1:0.75	1:1	1:2	1:5	1:10
Zeta Potential (mV)	-0.99	21.1	24.9	39.4	30.2	40.4	42	47.3	47.5
Standard Deviation (mV)	± 4.0	± 6.27	± 5.98	± 5.09	± 8.84	± 6.92	± 5.08	± 6.92	± 5.43

Fig. 4 Studying the hydrodynamic radius and charge using dynamic light scattering. (A) The hydrodynamic radius of mQDs in water as solvent has two sizes: 10.1 nm and 78 nm. (B) The hydrodynamic radius of DOTMA in water is 142 nm. (C) The hydrodynamic radius of the 1 : 0.25 ratio mQD : DOTMA conjugate is 122 nm. (D) The hydrodynamic radius of the 1 : 0.5 mQD : DOTMA conjugate is 122 nm. (E) The hydrodynamic radius of the 1 : 0.75 mQD : DOTMA conjugate is 122 nm. (F) The hydrodynamic radius of the 1 : 1 mQD : DOTMA conjugate is 122 nm. (G) The hydrodynamic radius of the 1 : 2 mQD : DOTMA conjugate is 164 nm. (H) The hydrodynamic radius of the 1 : 5 mQD : DOTMA conjugate is 190 nm. (I) The hydrodynamic radius of the 1 : 10 mQD : DOTMA conjugate is 190 nm. (J) The zeta potential of mQDs, DOTMA and their ratios (in mV).

filter. Quantum dots were formed. To obtain their powder a rotavapor was used as illustrated in Fig. 2.

The mQDs thus formed have an inherent negative charge, which prompted us to conjugate it electrostatically with the positively charged small lipid molecule *N*-[1-(2,3-dioleyloxy) propyl]-*N*,*N*,*N*-trimethylammonium chloride (DOTMA). The mQDs and DOTMA were mixed in the following ratios: 1 : 0.25, 1 : 0.5, 1 : 1, 1 : 2, 1 : 5 and 1 : 10, with water as the solvent. Next, characterization studies were carried out for the mQDs and the bioconjugates.

To characterize the quantum dots thus formed the optical properties were analyzed using UV spectra and fluorescence spectra. In UV spectra, for DOTMA there were no peaks observed, whereas peaks were observed in case of mQDs at 206 nm (–OH group) and 260 nm (flavonoids), and the mQD : DOTMA conjugate displayed both the peaks of mQDs and another peak at 327 nm as shown in Fig. 3(A). Further, for fluorescence spectra the 400 nm wavelength was chosen as it gave the maximum intensity. Fluorescence spectra of DOTMA showed a peak at 460 nm, and both mQDs and the mQD : DOTMA conjugate displayed peaks at 460 nm, 495 nm, 549 nm and 679 nm upon excitation at 400 nm as shown in Fig. 3(B). As the DOTMA concentration increased the fluorescence intensity of the sample increased (Fig. 3(B)). Hence, we observed the presence of DOTMA not only enhanced the fluorescence of mQDs but also increased the photostability of mQDs (ESI Fig. 1†). Next to understand the functional groups present on our quantum dots we performed FTIR, and the spectra show the presence of different functional groups present on the surface of mQDs: 2923 cm^{-1} for alkanes and acidic groups; 2850 cm^{-1} for aldehyde, alkanes, and acidic groups; 1560 cm^{-1} for nitro compounds; 1188 cm^{-1} for anhydride (acyl), amines, alcohol (alkoxy), and esters; and 938 cm^{-1} for alkenes (sp^2 C–H), as shown in Fig. 3(C).

To analyze the size and morphology of the quantum dots Atomic Force Microscopy (AFM) and Dynamic Light Scattering (DLS) were performed for both mQDs and mQD : DOTMA conjugates. The quasi-spherical morphology and topography of mQDs and DOTMA were observed with a size of about 30 nm and 179 nm, respectively (Fig. 3(D,E,G and H)). The ring-like structure of the DOTMA coating around the mQD can be observed in case of the conjugate and was about 580 nm (Fig. 3(F) and (I)).

mQDs and DOTMA were mixed in water as a solvent and the following ratios were made: 1 : 0.25, 1 : 0.5, 1 : 0.75, 1 : 1, 1 : 2, 1 : 5, 1 : 10. The hydrodynamic size and zeta potential were assessed following the conjugation of mQDs with DOTMA as shown in Fig. 4(A–I). The hydrodynamic size of mQDs and DOTMA alone in water as solvent was measured to be 10.1 nm and 142 nm, respectively. The hydrodynamic radius of mQDs : DOTMA (1 : 0.25, 1 : 0.5, 1 : 0.75, 1 : 1, 1 : 2, 1 : 5, 1 : 10) in water was measured to be 122 nm, 122 nm, 122 nm, 122 nm, 164 nm, 190 nm, and 190 nm respectively. The size of the conjugates 1 : 0.25, 1 : 0.5, 1 : 0.75 and 1 : 1 showed a similar size as the mQD surface is not yet saturated with the lipid layer of DOTMA and the lipid layer/coating is still forming. As the concentration increases further the size of the bioconjugate increases with an increase in concentration of DOTMA as a new lipid layer is formed. A similar trend is observed in 1 : 2, 1 : 5 and 1 : 10 ratios where the size of the bioconjugate is approximately 164 nm, 190 nm and 190 nm as the surface gets saturated with DOTMA. Another saturation is observed in ratios 1 : 5 and 1 : 10, as even on increasing the concentration to double the amount the hydrodynamic radius remains the same. The zeta potential of our negatively charged mQD molecule is −0.99 mV and that of positively charged DOTMA is 21.1 mV. We can observe an increase in the positive charge in the conjugates as the concentration of DOTMA increases as shown in Fig. 4(J).

3.2. Cytotoxic study of mQDs and mQDs : DOTMA

To investigate the cell-specific responses to mQDs and mQD : DOTMA, we conducted 3-[4,5-dimethylthiazol-2-yl]-2,5-diphenyltetrazolium bromide (MTT) assays on RPE1 epithelial cells and SUM159A breast cancer cells. The assay was done with increasing concentrations of mQDs (100, 200, 300 μg mL^{-1}) and 1 : 0.5, 1 : 1, 1 : 2, 1 : 5, and 1 : 10 ratios of mQD : DOTMA (100, 200, and 300 μg mL^{-1}) were administered to the cells. After a 24 hour incubation period, we calculated the percentage viability for both the cell types.

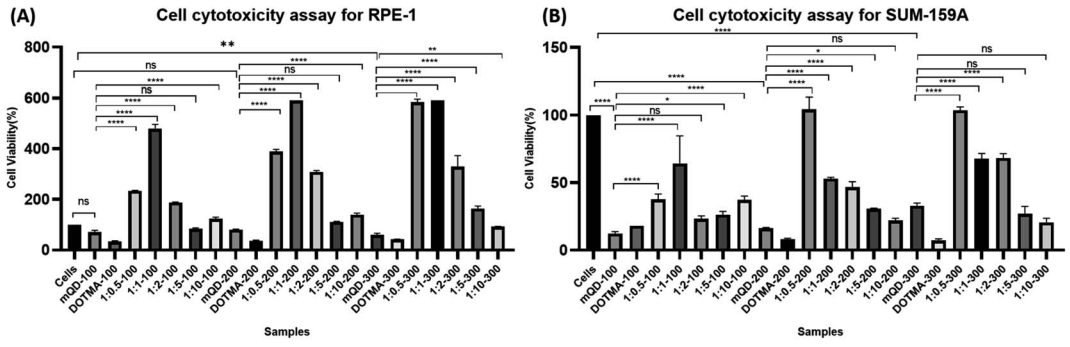

Fig. 5 Cytotoxicity assay: (A) treatment of different concentrations (100, 200 and 300 μg mL^{-1}) of mQDs, DOTMA and mQD : DOTMA biconjugate in SUM-159A and (B) treatment of different concentrations (100, 200 and 300 μg mL^{-1}) of mQDs, DOTMA and mQD : DOTMA biconjugate in RPE-1 cells. (The following thresholds were used when determining significance. ****$p < 0.0001$. ***$p < 0.001$. **$p < 0.01$. *$p < 0.05$. ns: $p > 0.05$ and denotes no significance.)

The SUM-159A cells with mQDs alone at concentrations of 100, 200, and 300 μg mL^{-1} showed cell viability of 12%, 16%, and 33% respectively. For SUM-159A cells with DOTMA alone at concentrations of 100, 200, and 300 μg mL^{-1} the corresponding values were 18%, 8%, and 8% respectively. This established that in SUM-159 cells mQDs alone and DOTMA alone are toxic to the cells and hence the cell viability has decreased significantly. For ratios 1 : 0.5, 1 : 1, 1 : 2, 1 : 5 and 1 : 10 concentrations 100, 200 and 300 μg mL^{-1} were taken. The cell viability for ratio 1 : 0.5 is 38%, 104%, and 104% respectively. The cell viability for ratio 1 : 1 is 64%, 53%, and 68% respectively. The cell viability for 1 : 2 is 23%, 47%, and 68% respectively. The cell viability for 1 : 5 is 26%, 30%, and 27% respectively. And for ratio 1 : 10 cell viability is 38%, 22%, and 21% respectively. Hence, we can see that the 1 : 0.5 ratio of mQD : DOTMA at 200 and 300 μg mL^{-1} concentrations is not toxic to the cell and can be further explored as a potential molecule for bioimaging purposes.

Further with respect to RPE cells, mQDs alone at 100, 200, and 300 μg mL^{-1} showed cell viability of 71%, 80%, and 60%. For DOTMA alone the cell viability is 33%, 37%, and 42%. These findings suggest that DOTMA when given alone to the cells is toxic. For ratios 1 : 0.5, 1 : 1, 1 : 2, 1 : 5 and 1 : 10 concentrations 100, 200 and 300 μg mL^{-1} were taken. The cell viability for ratio 1 : 0.5 is 150%, 252%, and 292% respectively. The cell viability for ratio 1 : 1 is 226%, 284%, and 370% respectively. The cell viability for 1 : 2 is 227%, 315%, and 353% respectively. The cell viability for 1 : 5 is 83%, 111%, and 164% respectively. And for ratio 1 : 10 cell viability is 123%, 139%, and 92% respectively. We can see that when mQDs are conjugated with DOTMA they quench the cytotoxic effect and further lead to cell proliferation as seen in Fig. 5.

3.3. Cellular uptake of mQDs and mQDs : DOTMA

After characterization, these mQDs and mQD : DOTMA conjugates were employed to examine their impact on cell lines. Their effects were assessed on SUM-159A cancerous cells, considering previous reports indicating the anti-cancer properties of mQDs. Fluorescence signals emitted by mQDs, alongside standard markers like DAPI (for the nucleus), aided in visualizing cellular

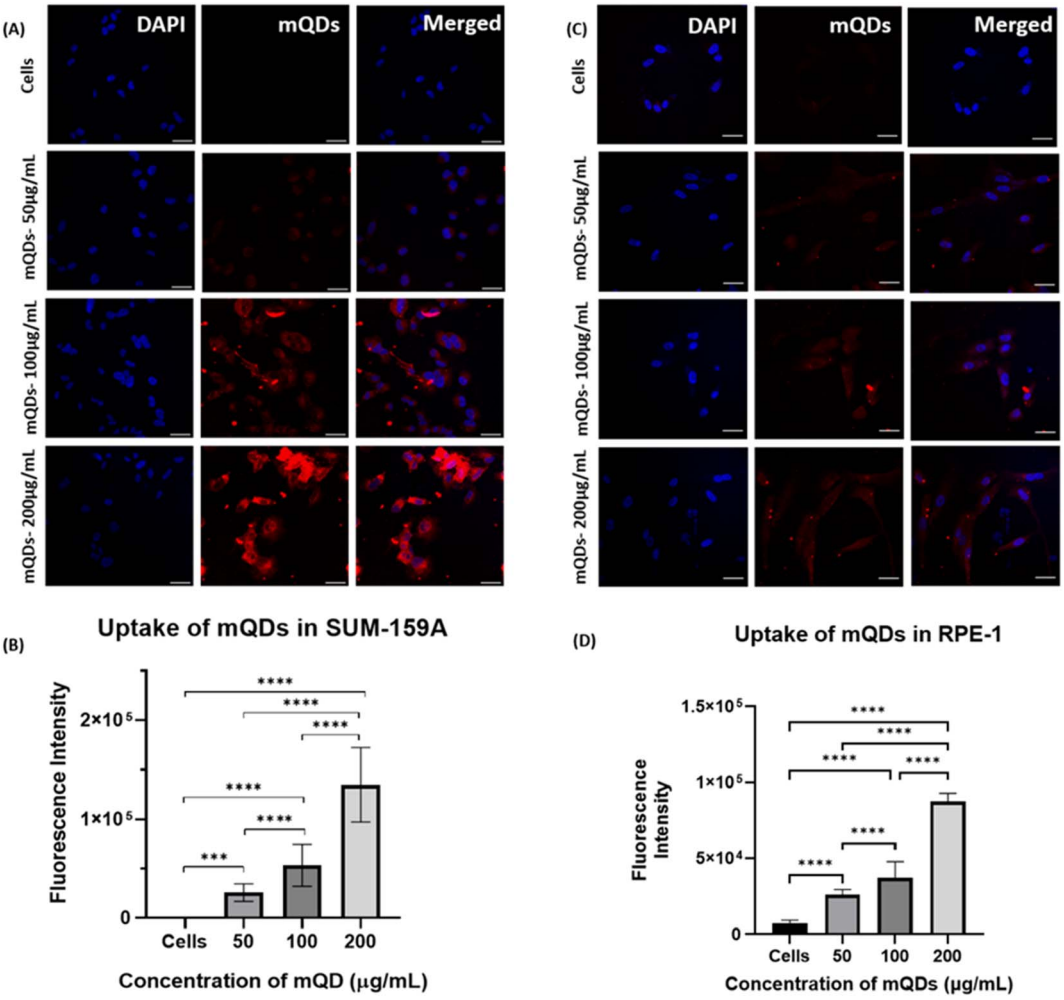

Fig. 6 Cellular uptake of mQDs in SUM-159A and RPE-1. Scale bar 5 μm. (A) Uptake of mQDs at concentrations of 50 μg mL^{-1}, 100 μg mL^{-1}, and 200 μg mL^{-1} in SUM-159A. (B) Quantified fluorescence intensity of mQDs in SUM-159A. (C) Uptake of mQDs at concentrations of 50 μg mL^{-1}, 100 μg mL^{-1}, and 200 μg mL^{-1} in RPE-1. (D) Quantified fluorescence intensity of mQDs in RPE-1. The statistical significance was tested by one-way ANOVA in the Prism Software and is represented as **** when $p < 0.0001$ and ns when there is no significant difference ($n = 30$).

morphology and physiology. Based on the toxicity studies, two experiments were designed to validate our results. Two types of cells were taken for the study, namely cancer cells (SUM159A) and non-cancerous epithelial cells (RPE-1). The cells were seeded and later treated with mQDs and mQDs : DOTMA to observe the effect.

In the case of both cancer cells and epithelial cells, there was an increase in uptake at concentrations of 100 and 200 μg mL^{-1} of mQDs compared to 50 μg mL^{-1} and control. Thus, the cellular uptake studies were performed with 100 μg mL^{-1} and 200 μg mL^{-1} concentrations as shown in Fig. 6.

Further uptake studies for mQD : DOTMA conjugates were done both in SUM-159 and RPE-1 cells using concentrations of 100 μg mL^{-1} and 200 μg mL^{-1}. The uptake of bioconjugates as compared to mQDs when provided alone was less in both the cell lines. This could be due to the highly positive charge on the conjugates and the increase in size, which might lead to a decrease in the uptake. Upon comparing the ratios in SUM-159A cancerous cells, we can observe that in case of 100 μg mL^{-1} concentration, a 1 : 2 ratio has relatively higher uptake as compared to others as shown in Fig. 7. A similar trend was observed in case of 200 μg mL^{-1} where the mQD : DOTMA bioconjugate's fluorescence intensity was lower indicating lower uptake of the molecule in the cytoplasm as shown in ESI Fig. S2.† Comparing the ratios, we found comparably higher uptake of both 1 : 2 and 1 : 10 ratios.

In the case of non-cancerous epithelial cells RPE-1, the uptake of the mQD : DOTMA conjugate is relatively lower than only mQDs which can be due to the increase in size and positive charge on the bioconjugate. When the cells are treated with 100 μg mL^{-1} concentration of mQD : DOTMA, there was an increase in fluorescence intensity in 1 : 5 and 1 : 10 which indicates an increase in cellular uptake as shown in Fig. 8. And when the cells were treated with 200 μg mL^{-1} concentration of mQD : DOTMA, similar results were obtained (ESI Fig. S3†).

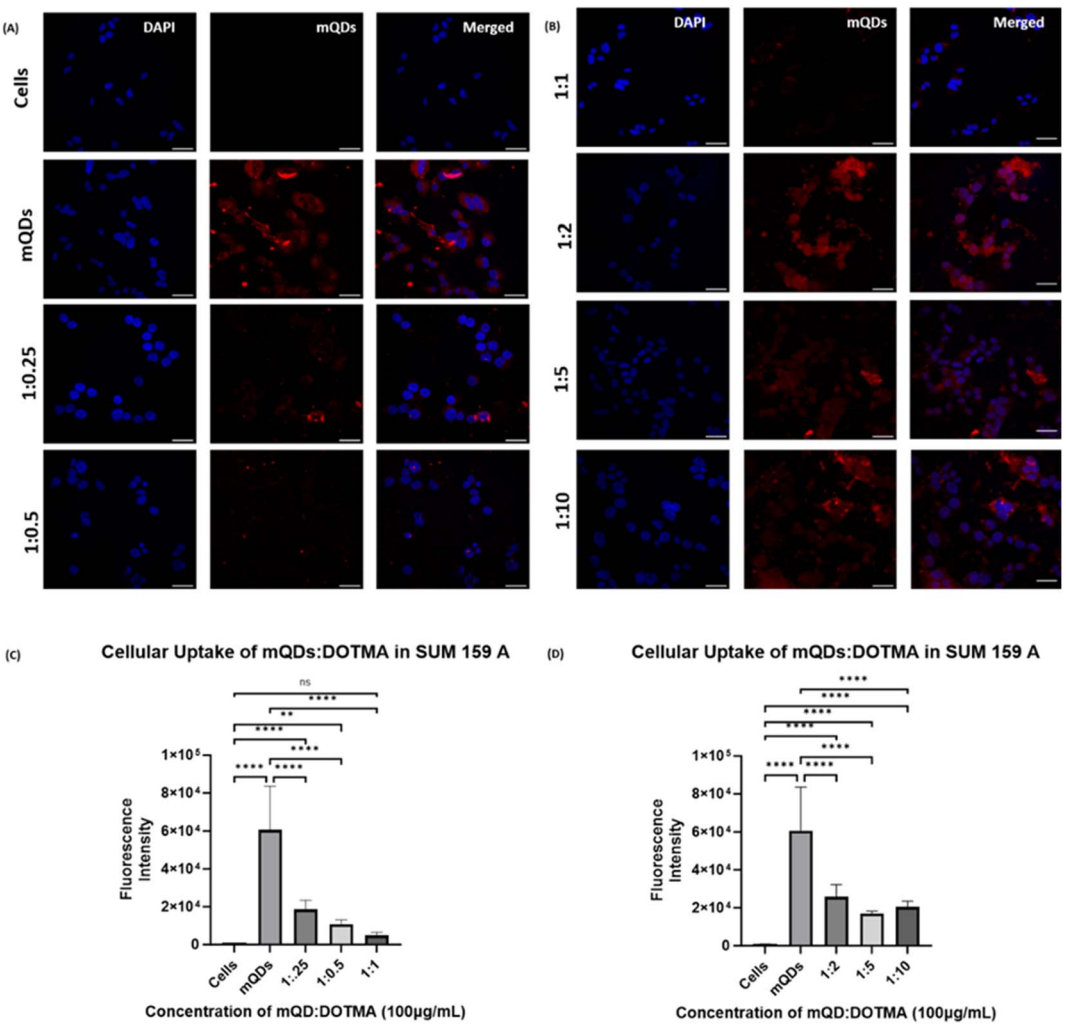

Fig. 7 Cellular uptake of mQD : DOTMA conjugates in SUM-159A cells. Concentration – 100 μg mL^{-1}, scale bar 5 μm. (A) Uptake of mQDs and the mQD : DOTMA conjugate (1 : 0.25 and 1 : 0.5). (B) Uptake of the mQD : DOTMA conjugate (1 : 1, 1 : 2, 1 : 5, 1 : 10). (C) Quantified fluorescence intensity of mQDs and mQD : DOTMA conjugates (1 : 0.25, 1 : 0.5, 1 : 1). (D) Quantified fluorescence intensity of mQD : DOTMA conjugates (1 : 2, 1 : 5, 1 : 10). The statistical significance was tested by one-way ANOVA in the Prism Software and is represented as **** when $p < 0.0001$ and ns when there is no significant difference ($n = 30$).

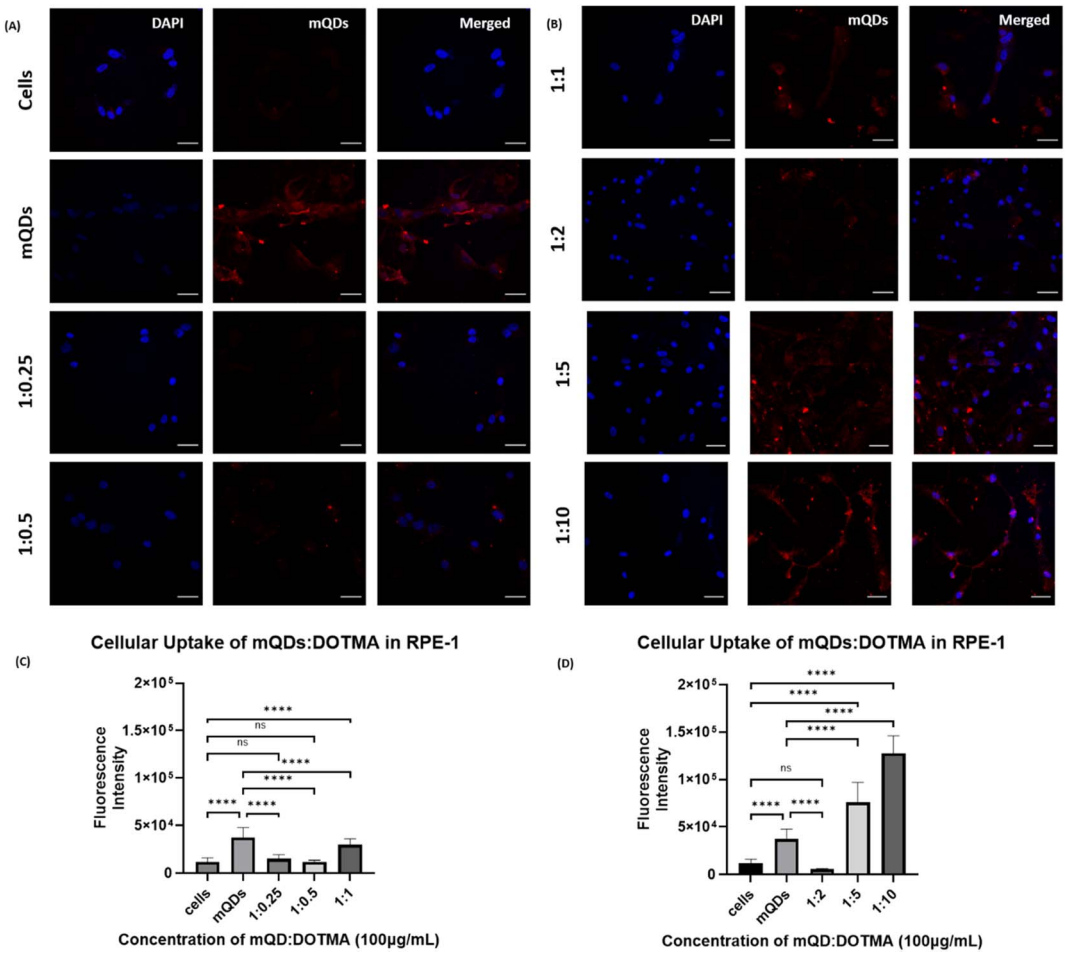

Fig. 8 Cellular uptake of mQD : DOTMA conjugates in RPE-1 cells. Concentration – 100 µg mL^{-1}, scale bar 5 µm. (A) Uptake of mQDs and mQD : DOTMA conjugate (1 : 0.25 and 1 : 0.5). (B) Uptake of the mQD : DOTMA conjugate (1 : 2, 1 : 5, 1 : 10). (C) Quantified fluorescence intensity of mQDs and mQD : DOTMA conjugates (1 : 0.25, 1 : 0.5, 1 : 1). (D) Quantified fluorescence intensity of mQD : DOTMA conjugates (1 : 2, 1 : 5, 1 : 10). The statistical significance was tested by one-way ANOVA in the Prism Software and is represented as **** when $p < 0.0001$ and ns when there is no significant difference ($n = 30$).

4. Conclusions and discussion

In this study, we have successfully synthesized red-emitting carbon quantum dots (mQDs) *via* a green synthesis approach, offering a sustainable and environmentally friendly method for producing versatile fluorescent probes (Fig. 2). These negatively charged mQDs were subsequently conjugated with a small cationic lipid molecule, DOTMA, through electrostatic interaction, resulting in the formation of bioconjugates with various mQD : DOTMA ratios – 1 : 0.25, 1 : 0.5, 1 : 0.75, 1 : 1, 1 : 2, 1 : 5, 1 : 10. Later, characterization analyses were carried out to confirm the conjugation and understand the properties of the biconjugate, including dynamic light scattering for size and zeta potential, UV-Vis spectroscopy, FTIR, fluorescence spectroscopy, and atomic force microscopy (AFM), which revealed the conjugation of mQDs with DOTMA (Fig. 3 and 4). The bioconjugate thus formed showed a significant increase in fluorescence intensity and photostability compared to standalone mQDs (Fig. 3B and ESI Fig. 1†). The AFM images also confirmed the successful conjugation of DOTMA with mQDs, showing distinct morphology changes, such as ring-like formation, consistent with the formation of the bioconjugate (Fig. 3F).

Next, we studied the effect of this biconjugate *in vitro* in cancerous cells (SUM-159A) and epithelial cells (RPE-1). Interestingly, our cellular uptake studies using fluorescence microscopy demonstrated that the uptake of the mQDs : DOTMA bioconjugate in SUM-159 (cancerous cells) was lower than that of mQDs alone (Fig. 7 and ESI Fig. S2†). This reduced uptake can be attributed to the increased size and zeta potential of the bioconjugates, which may hinder their cellular internalization[23] (Fig. 9). However, mQD : DOTMA bioconjugates with specific ratios showed higher uptake in RPE-1 cells, suggesting a potential dose-dependent effect on cellular internalization. Upon comparing different ratios of mQD : DOTMA, we found that in SUM-159A, the 1 : 2 and 1 : 10 ratios exhibited relatively higher uptake compared to others at both the concentrations of 100 and 200 µg mL^{-1}, as depicted in Fig. 7. Similarly, for RPE-1 the fluorescence intensity of the mQD : DOTMA conjugates of ratios 1 : 5 and 1 : 10 is higher than that of mQDs at both the

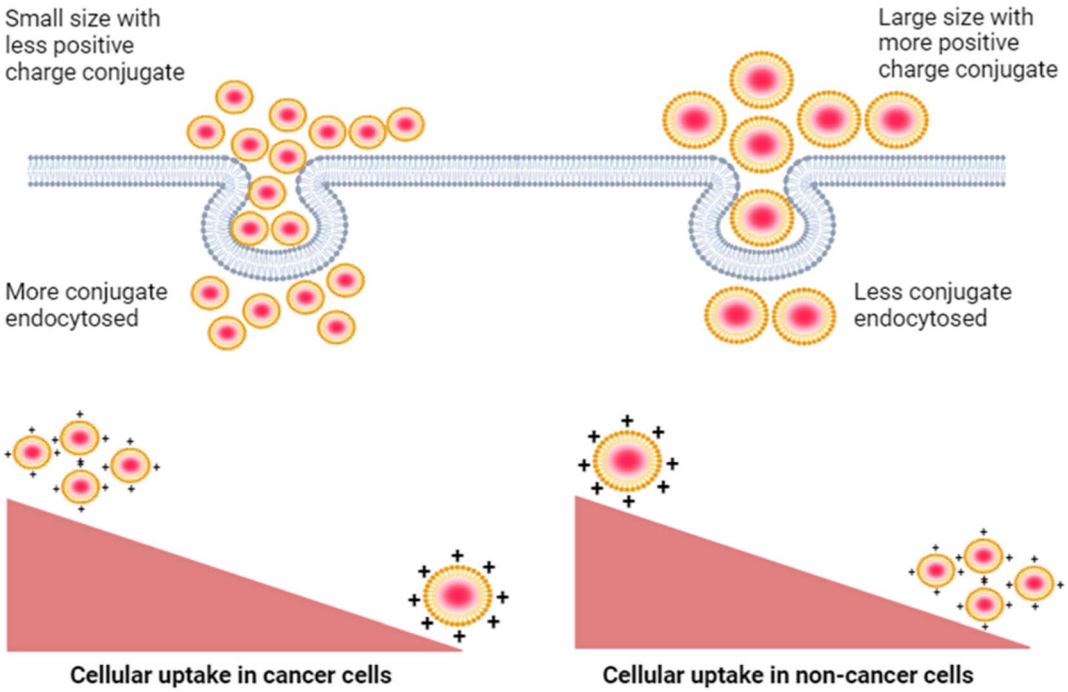

Fig. 9 Decreased cellular uptake of the mQD–DOTMA bioconjugate in cancer cells as compared to non-cancer cells due to increased size and zeta potential of the bioconjugate.

concentrations of 100 and 200 μg mL^{-1}, indicating increased cytoplasmic uptake, as illustrated in Fig. 8 and ESI Fig. S2.†

Furthermore, cytotoxicity assays revealed that while both mQDs and DOTMA alone exhibited toxicity across all tested concentrations (100, 200, and 300 μg mL^{-1}) in SUM-159A and RPE-1 cells,[24] some ratios of the mQD : DOTMA bioconjugate showed quenching of cytotoxicity of individual molecules and maintained high cell viability. In SUM-159A 1 : 0.5 at concentrations of 200 and 300 μg mL^{-1} showed cell viability of 104% and 104% respectively. In RPE cells these bioconjugates have increased the cell viability. The maximum cell viability was observed in 1 : 2 at 100 μg mL^{-1} (cell viability 227%), 1 : 2 at 200 μg mL^{-1} (cell viability 315%) and 1 : 1 at 300 μg mL^{-1} (cell viability 370%). This indicates the potential of these bioconjugates to mitigate cytotoxic effects which can be further explored in bioimaging and potential therapeutics (Fig. 5).

The versatility of mQD : DOTMA bioconjugates opens up numerous possibilities for biomedical applications, including targeted drug delivery, cellular imaging, and therapeutics. The enhanced fluorescence intensity and photostability make them ideal candidates for sensitive and prolonged imaging of cellular processes. Furthermore, the ability to modulate cytotoxicity through ratio optimization underscores their potential as safe and effective drug delivery systems.

In conclusion, the mQD : DOTMA bioconjugates represent a promising platform for a wide range of biomedical applications, offering enhanced fluorescence properties, tunable cytotoxicity, and potential therapeutic benefits. Future studies should focus on further optimizing the bioconjugate ratios, investigating their efficacy *in vivo*, and exploring additional characterization techniques to fully realize their translational potential in biomedical research and clinical practice. This shows that the bioconjugate is not toxic and can be used in therapeutics.

Data availability

The data is available on request from the authors.

Author contributions

DB and PY conceptualized the idea. Sweny and Nidhi conducted the cellular uptake study, cell viability assay, data analysis, data plotting and manuscript writing. PY helped in mQD synthesis, conjugation, confocal microscopy, UV-Vis and fluorescence spectroscopy, DLS and AFM analysis.

Conflicts of interest

There are no conflicts to declare.

Acknowledgements

The authors sincerely thank all the members of the D. B. group for critically reading the manuscript and for their valuable feedback. P. Y. thanks IITGN-MHRD, GoI, for the PhD fellowship; P. Y. acknowledges the Director's fellowship from IITGN for additional fellowship. D. B. thanks SERB, GoI for the Ramanujan Fellowship, DST-Nidhi Prayas for the start-up grant, and Gujcost-DST, GSBTM, BRNS-BARC, and HEFA-GoI, MoES for STARS for research grants. D. B. is a member of the Indian

National Young Academy of Sciences (INYAS). CIF at IIT Gandhinagar for confocal and AFM facility, Prof. Chinmay Ghoroi and the CRTDH lab in the Chemical Engineering department at IITGN for fluorescence studies, and the DLS and FTIR facility in the Materials Science department at IITGN are acknowledged.

References

1 M. Kumar, V. Saurabh, M. Tomar, M. Hasan, S. Changan, M. Sasi, *et al.*, Mango (Mangifera indica L.) Leaves: Nutritional Composition, Phytochemical Profile, and Health-Promoting Bioactivities, *Antioxidants*, 2021, **10**(2), 299.

2 P. Yadav, D. Benner, R. Varshney, K. Kansara, K. Shah, L. Dahle, *et al.*, Dopamine-Functionalized, Red Carbon Quantum Dots for *In Vivo* Bioimaging, Cancer Therapeutics, and Neuronal Differentiation, *ACS Appl. Bio Mater.*, 2024, **7**(6), 3915–3931.

3 S. Kargozar, S. J. Hoseini, P. B. Milan, S. Hooshmand, H. Kim and M. Mozafari, Quantum Dots: A Review from Concept to Clinic, *Biotechnol. J.*, 2020, **15**(12), 2000117.

4 A. V. Longo, A. Sciortino, M. Cannas and F. Messina, UV photobleaching of carbon nanodots investigated by *in situ* optical methods, *Phys. Chem. Chem. Phys.*, 2020, **22**(24), 13398–13407.

5 J. F. Galloway, A. Winter, H. L. Kwan, J. Ho Park, C. M. Dvoracek, P. Devreotes, *et al.*, Quantitative characterization of the lipid encapsulation of quantum dots for biomedical applications, *Nanomed. Nanotechnol. Biol. Med.*, 2012, **8**(7), 1190–1199.

6 P. K. Yadav, S. Chandra, V. Kumar, D. Kumar and S. H. Hasan, Carbon Quantum Dots: Synthesis, Structure, Properties, and Catalytic Applications for Organic Synthesis, *Catalysts*, 2023, **13**(2), 422.

7 P. Devi, S. Saini and K. H. Kim, The advanced role of carbon quantum dots in nanomedical applications, *Biosens. Bioelectron.*, 2019, **141**, 111158.

8 M. Pourmadadi, E. Rahmani, M. Rajabzadeh-Khosroshahi, A. Samadi, R. Behzadmehr, A. Rahdar, *et al.*, Properties and application of carbon quantum dots (CQDs) in biosensors for disease detection: A comprehensive review, *J. Drug Delivery Sci. Technol.*, 2023, **80**, 104156.

9 L. Tian, Z. Li, P. Wang, X. Zhai, X. Wang and T. Li, Carbon quantum dots for advanced electrocatalysis, *J. Energy Chem.*, 2021, **55**, 279–294.

10 L. Cui, X. Ren, M. Sun, H. Liu and L. Xia, Carbon Dots: Synthesis, Properties and Applications, *Nanomaterials*, 2021, **11**(12), 3419.

11 E. Muro, G. E. Atilla-Gokcumen and U. S. Eggert, Lipids in cell biology: how can we understand them better?, *Molecular Biology of the Cell*, ed. W. Bement. 2014, vol. 25, 12, pp. 1819–1823, Available from: **https://www.ncbi.nlm.nih.gov/pmc/articles/PMC4055261/**.

12 T. Harayama and H. Riezman, Understanding the diversity of membrane lipid composition, *Nat. Rev. Mol. Cell Biol.*, 2018, **19**(5), 281–296.

13 J. Park, J. Choi, D. D. Kim, S. Lee, B. Lee, Y. Lee, *et al.*, Bioactive Lipids and Their Derivatives in Biomedical Applications, *Biomol. Ther.*, 2021, **29**(5), 465–482. **https://www.biomolther.org/journal/view.html?uid=1353&vmd=Full**.

14 A. Luchini and G. Vitiello, Understanding the Nano-bio Interfaces: Lipid-Coatings for Inorganic Nanoparticles as Promising Strategy for Biomedical Applications, *Front. Chem.*, 2019, **7**, DOI: **10.3389/fchem.2019.00343**.

15 Y. Jiang, W. Li, Z. Wang and J. Lu, Lipid-Based Nanotechnology: Liposome, *Pharmaceutics*, 2023, **16**(1), 34–44. **https://www.ncbi.nlm.nih.gov/pmc/articles/PMC10820119/**.

16 R. Singh, P. Yadav, N. Hema and D. D. Bhatia, Cationic lipid modification of DNA tetrahedral nanocages enhances their cellular uptake, *Nanoscale*, 2023, **15**(3), 1099–1108.

17 H. C. Huang, P. Y. Chang, K. Chang, C. Y. Chen, C. W. Lin, J. H. Chen, *et al.*, Formulation of novel lipid-coated magnetic nanoparticles as the probe for in vivo imaging, *J. Biomed. Sci.*, 2009, **16**(1), 86.

18 H. Yasar, A. Biehl, C. De Rossi, M. Koch, X. Murgia, B. Loretz, *et al.*, Kinetics of mRNA delivery and protein translation in dendritic cells using lipid-coated PLGA nanoparticles, *J. Nanobiotechnol.*, 2018, **16**(1), 72.

19 D. B. Tada, E. Suraniti, L. M. Rossi, C. A. P. Leite, C. S. Oliveira, T. C. Tumolo, *et al.*, Effect of Lipid Coating on the Interaction Between Silica Nanoparticles and Membranes, *J. Biomed. Nanotechnol.*, 2014, **10**(3), 519–528. **https://pubmed.ncbi.nlm.nih.gov/24730247/**.

20 S. J. H. Soenen, A. R. Brisson and M. De Cuyper, Addressing the problem of cationic lipid-mediated toxicity: The magnetoliposome model, *Biomaterials*, 2009, **30**(22), 3691–3701.

21 X. Lin and T. Chen, A Review of in vivo Toxicity of Quantum Dots in Animal Models, *Int. J. Nanomed.*, 2023, **18**, 8143–8168.

22 J. Qi, J. Zhuang, Y. Lu, X. Dong, W. Zhao and W. Wu, In vivo fate of lipid-based nanoparticles, *Drug Discovery Today*, 2017, **22**(1), 166–172. **https://pubmed.ncbi.nlm.nih.gov/27713035/**.

23 C. He, Y. Hu, L. Yin, C. Tang and C. Yin, Effects of particle size and surface charge on cellular uptake and biodistribution of polymeric nanoparticles, *Biomaterials*, 2010, **31**(13), 3657–3666.

24 E. Winter, C. Dal Pizzol, C. Locatelli and T. B. Crezkynski-Pasa, Development and Evaluation of Lipid Nanoparticles for Drug Delivery: Study of Toxicity In, Vitro and In Vivo, *J. Nanosci. Nanotechnol.*, 2016, **16**(2), 1321–1330. **https://pubmed.ncbi.nlm.nih.gov/27433582/**.